

Article

Hydrodynamic Drivers of Nutrient and Phytoplankton Dynamics in a Subtropical Reservoir

Mayra Ishikawa ^{1,*}, Luziadne Gurski ², Tobias Bleninger ² , Harald Rohr ³, Nils Wolf ⁴ and Andreas Lorke ¹ 

¹ Institute for Environmental Sciences, University of Koblenz-Landau, 76829 Landau, Germany; lorke@uni-landau.de

² Graduate Program in Water Resources and Environmental Engineering, Federal University of Paraná, Curitiba 82590-300, Brazil; luziadne@ufpr.br (L.G.); bleninger@ufpr.br (T.B.)

³ TriOS Mess- und Datentechnik GmbH, 26180 Rastede, Germany; rohr@trios.de

⁴ EFTAS GmbH, 48145 Münster, Germany; nils.wolf@eftas.com

* Correspondence: ishikawa@uni-landau.de

Abstract: Chlorophyll-a (chl_a) is an important parameter to assess water quality in lakes and reservoirs, since it is a proxy for phytoplankton biomass and primary production. The increasing availability of data with high spatial and temporal resolution allows assessing short-term dynamics and small-scale variations of chl_a within larger water bodies. In freshwater reservoirs, the nutrient concentrations and the physical conditions that control phytoplankton growth vary along their longitudinal extend. Here, we analyze how the flow paths of the inflowing river water into density-stratified reservoirs affect the vertical and longitudinal distribution of nutrients and chl_a. We combine spatially resolved and high-frequency measurements of chl_a from satellite remote sensing and in-situ sensors, with numerical simulations using a three-dimensional hydrodynamic model to assess the influence of density currents on chl_a dynamics along a subtropical drinking water reservoir in the south of Brazil. Chl_a did not have pronounced seasonal dynamics ($4.9 \pm 1.2 \mu\text{g L}^{-1}$, at the continuous measurement station); instead, spatial variability along the reservoir was more pronounced ($4.4 \pm 2.1 \mu\text{g L}^{-1}$, all monitored points within the euphotic zone). Most of the nutrients from the inflowing river were consumed in the upstream region, and phytoplankton in the lacustrine zone depended on internal loading. Temporal variability was observed only in the upstream region, and phytoplankton produced in that area was transported downstream by density currents, resulting in large concentrations of chl_a below the euphotic zone. The results of a hydrodynamic model that simulates the present state are in good agreement with the observations. Two simulated scenarios, where the density current patterns were altered, resulted only in slight variations in density currents, indicating that the influence of the main inflow was of minor relevance in chl_a concentrations in downstream regions of the reservoir. Our results highlight the importance of two-dimensional hydrodynamic processes in regulating phytoplankton dynamics in reservoirs.

Keywords: water quality; reservoirs; chlorophyll-a; nutrients; density currents



Citation: Ishikawa, M.; Gurski, L.; Bleninger, T.; Rohr, H.; Wolf, N.; Lorke, A. Hydrodynamic Drivers of Nutrient and Phytoplankton Dynamics in a Subtropical Reservoir. *Water* **2022**, *14*, 1544. <https://doi.org/10.3390/w14101544>

Academic Editors: Roohollah Noori, Rabin Bhattacharai and Soroush Abolfathi

Received: 20 April 2022

Accepted: 7 May 2022

Published: 11 May 2022

Publisher's Note: MDPI stays neutral with regard to jurisdictional claims in published maps and institutional affiliations.



Copyright: © 2022 by the authors. Licensee MDPI, Basel, Switzerland. This article is an open access article distributed under the terms and conditions of the Creative Commons Attribution (CC BY) license (<https://creativecommons.org/licenses/by/4.0/>).

1. Introduction

The water quality in lakes and reservoirs is often assessed by the concentration of chlorophyll-a (chl_a), which is a proxy of the biomass and primary production of phytoplankton, and an important parameter for determining the index of trophic state [1,2]. For this reason, the prediction of chl_a is essential for the management of inland waters. Linear relationships between the concentration of total phosphorus in water and chl_a have been observed for many lakes [3,4]. Therefore, it became common practice to predict chl_a in lakes and reservoirs based on linear models using total phosphorus as a predictor [4–7]. Such relationships have been continuously revisited, due to the increasing amount of data and better approaches that can provide more robust estimates. For example, Stow and Cha [7] suggested that linear relationships would only hold for lakes with similar features. Most

recently, Quinlan, et al. [8] estimated that total phosphorus explained 44% of chl_a variation among 3874 lakes across 47 countries, though most of them were located in North America and Europe. A sigmoidal relationship was found between the two parameters, and the regions where the linear relationship was not valid were in either most cold or hot climates. Similarly, existing studies show that the linear relationships are rather poor predictors for chl_a in lakes located at low latitudes [9], and that the relationships between both parameters are not strictly linear [10]. Shuvo, et al. [11] demonstrated that additional factors can be relevant for chl_a, such as regional climate and the morphology of the water body. Most of the relationships between chl_a and total phosphorus were estimated using data from lakes, which are most abundant at higher latitudes [12], whereas there is a general lack of limnological studies in tropical and subtropical regions [13].

Freshwater reservoirs have been constructed globally for different purposes, with recent estimates suggesting a number of 38,000 existing dams [14]. Hotspots for the ongoing construction and planning of new dams are located in tropical zones [15]. Water quality in reservoirs has become a global concern, particularly in drinking water reservoirs, where their degradation caused by eutrophication and rising temperature may abate the services that they provide [16–18]. In distinction to lakes, reservoirs can be divided into three distinct zones along their longitudinal extent from the inflow region to the dam, namely the riverine, transitional, and the lacustrine zone. These zones differ in temperature, underwater light availability, turbidity, and nutrient concentration [19]. For this reason, the spatial variations and dynamics of primary production in reservoirs differs from natural lakes, although the drivers are identical [20]. According to Kimmel, Lind, and Paulson [19], nutrient availability, suspended particle concentration, and light limitation in reservoirs decrease toward the dam. Therefore, phytoplankton production has its maximum in the transition zone, where nutrients are still largely available and light limitation is reduced due to sedimentation of suspended particles. In the lacustrine zone, light and flow conditions are more favorable for phytoplankton growth, but the nutrients are limited, and growth depends on internal loading, i.e., from the release of remineralized nutrients from the sediment. In addition, besides nutrient loads, factors such as the hydraulic residence time have an impact on the trophic state of reservoirs [21].

The relationships between total phosphorus and chl_a have mostly been analyzed using longer-term data and for annual mean values of measurements obtained at a single location or for the average of several sampling points (e.g., [7,8]). The increasing availability of data with high spatial and temporal resolution, however, also lead to usage of trophic state indices to explain short-term dynamics and small-scale variations within larger water bodies (e.g., [22]). Remote sensing techniques have become useful tools to monitor and evaluate the quality of inland waters, measuring qualitative parameters of water with spatial and temporal variations [23].

For assessing spatial variations and temporal dynamics, the hydrodynamic conditions and, in the case of reservoirs, longitudinal gradients need to be taken into account. The flow path of inflowing waters into density-stratified reservoirs can be classified according to its depth distribution. The vertical position of the inflow depends on reservoir stratification and the density of the inflowing water, which enters at a depth of neutral buoyancy. Accordingly, the density currents are defined as under-, inter-, and overflows, where in the first the river, water flows along the reservoir bottom, in the second at an intermediate water depth, and in the latter along the water surface. The potential importance of density currents for reservoir water quality has been analyzed in recent years [24–26]. These studies addressed the hypothesis that overflows and interflows promote the growth of phytoplankton, as they can deliver nutrients directly to the euphotic zone.

The aim of the present study is to analyze the role of reservoir hydrodynamics for the longitudinal variations and the temporal dynamics of the relationships between nutrient concentration and chl_a in a subtropical reservoir. We combine spatially resolved and high-frequency measurements of chl_a from satellite remote sensing and in-situ sensors, with numerical simulations using a three-dimensional hydrodynamic model. We analyze

to what extent nutrient concentration and prevailing density currents can explain the dynamics of chl a in different regions along the reservoir. In addition, we assessed two scenarios for projected changes of density currents due to changing inflow temperature and changing reservoir morphology. Our results provide information about the applicability of fixed relationships between nutrient concentration and water quality in reservoirs located at low latitude, and advance the understanding of the role of physical processes in these relationships.

2. Methods

2.1. Study Site

The study site is a drinking water reservoir located in a subtropical region in South Brazil at latitude 25.50° S. Passaúna Reservoir is of small to medium size and used for the abstraction of on average $1.8 \text{ m}^3 \text{ s}^{-1}$ of potable water for about one half million people (Sanitation Company of Paraná—SANEPAR [27]). The maximum water depth close to the dam is 17.5 m, the surface area is 8.5 km^2 , and it has a storage volume of $48 \times 10^6 \text{ m}^3$. In the upstream region of the reservoir, a forebay was formed due to the presence of a bridge (Figure 1). The main inflow is the Passaúna River that represents, on average, 77% of all incoming discharge. The outflows are the bottom outlet at the dam that had a continuous discharge of $\sim 0.5 \text{ m}^3 \text{ s}^{-1}$, the spillway at the dam, and the intake for the water treatment plant. Data on air temperature and wind speed are available from two stations. Until May 2018, data were provided by the Technology Institute of Paraná (TECPAR), located 4 km from the reservoir in the east direction. After that, measurements were provided by a station near to the dam and operated by SANEPAR. Both stations provided observations with a temporal resolution of 10 min. Precipitation was measured at the dam station for the entire period.

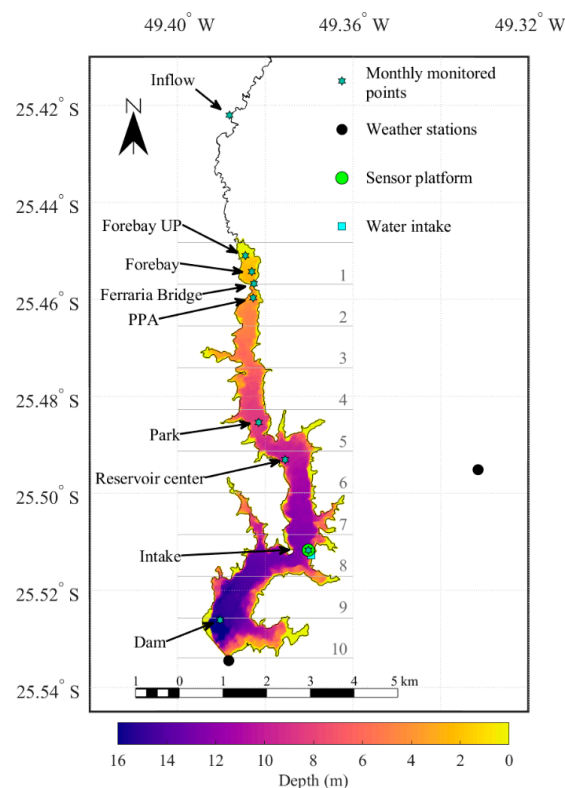


Figure 1. Map of Passaúna Reservoir. The color map shows the reservoir bathymetry (adopted from Sotiri, et al. [28]); the location of the dam, the intake station, and the main river inflow are indicated by text labels. Symbols mark the location of sampling sites for continuous sensor observations and monthly water quality sampling (see legend). The latitudinal sections (numbered as 1 to 10) are used in the spatial analysis of model simulations and remote sensing data.

2.2. Monitoring Program

Passaúna Reservoir was monitored for one year, starting from February 2018. The monitoring program was composed of three extensive and seven smaller sampling campaigns; the latter had fewer sampling locations along the reservoir. Water sampling and in-situ measurements with sensors were performed from 3 to 10 sampling sites during seven campaigns, and additional continuous sensor measurements along longitudinal, a transect crossing the complete reservoir, were measured during the three extensive campaigns. In addition to the sampling campaigns, continuous sensor measurements of surface water properties were obtained at a fixed platform near the water intake (Figure 1). The sampling schedule and the location and water depths of the measurements conducted during the campaigns are provided in Table S1. Detailed descriptions of sensor measurements and water sample analyses are provided in the following sections. In addition, Secchi disk depth (z_{SD}) was measured at each location, which were used to estimate euphotic zone depths (z_e) following Luhtala and Tolvanen [29]:

$$z_e = 3.7489 \times z_{SD}^{0.7506} \quad (1)$$

2.2.1. Sensors

Several sensors were used to measure vertical profiles at the selected sampling locations, for measuring longitudinal transects at the reservoir surface, and for continuous time series at the platform location (Table 1).

Table 1. Sensor's specification regarding variables measured, type of measurement, range, accuracy, and temporal resolution.

Equipment	Fluorometer	Spectrometer	Fluorometer	Conductivity, Temperature, and Depth Profiler
Equipment model	nanoFlu	OPUS	FluoroProbe III	CastAway-CTD
Manufacturer	TriOS	TriOS	bbe moldaenke	Sontek
Origin	Rastede, Germany	Rastede, Germany	Schwentinental, Germany	San Diego, United States
Variables measured	chl _a	Nitrate(N-NO ₃)	chl _a with the determination of algae classes	conductivity, temperature, and depth
Range	0 to 200 µg L ⁻¹	0.03 to 10 mg L ⁻¹	0 to 500 µg L ⁻¹	
Accuracy/Resolution	±5%	±5%	0.01 µg L ⁻¹	0.1 PSU and 0.05 °C
Measurements	continuous time series	continuous time series	continuous time series, longitudinal transects, and vertical profiles	Vertical profiles
Temporal resolution	15 min	15 min	for continuous measurement 1 h, and 1 s for transects and profiles	Sampling in a rate of 5 Hz.

OPUS is an UV spectral sensor that, through the analysis of the full spectrum, determines concentrations of nitrate (N-NO₃). Both nanoFlu and the FluoroProbe (bbe moldaenke) are fluorometers; however, the last one makes the assessment of chl_a with the determination of five different algae classes.

Fluorometer-based measurements potentially underestimate chl_a concentration in the presence of daylight due to photochemical quenching [30], which was observed in our measurements with both chl_a probes. For this reason, data acquired between 8 am and 8 pm were excluded from the continuous measurements at the platform, and the remaining data were averaged to provide daily estimates of chl_a. The sensor data were

calibrated using a linear regression of daily averaged sensor data and the data obtained from laboratory analysis of water samples collected during the campaigns (Figure S1). The factory calibrations resulted in averaged overestimations of a factor of 1.46 for the nanoFlu, and 2.13 for the FluoroProbe. The same correction was applied for measurements done during campaigns, even though they were performed during daytime. Measurements of N-NO₃ made with the sensor were in good agreement with laboratory analyses (Figure S2).

2.2.2. Laboratory Analyses

Water samples were collected during the campaigns at each sampling site (Figure 1) using a Van Dorn sampler. The sampled depths included the water surface (0.2 m depth), the near-bottom layer (~0.5 m above the bottom), and up to three additional depths according to the measured temperature stratification (Table S1). The sampling depths were defined after the assessment of the temperature profile to resolve the vertical gradients sufficiently. Polyethylene bottles were used for sample collection of chl_a analyses, and glass bottles for nutrient analysis. Chl_a samples were stored in darkness until analysis in the laboratory.

Chemical analyses of water samples included total nitrogen (TN), organic nitrogen (Organic N), ammonium (N-NH₄), nitrate (N-NO₃), nitrite (N-NO₂), total phosphorus (TP), total dissolved phosphorus (TDP), particulate phosphorus (particulate P), orthophosphate (P-PO₄), and chl_a. Sampling, preservation, and analytical protocols were following standard methods for surface waters [31].

Samples for TN and TP determination were kept unfiltered, and the remaining samples were filtered using a 0.45-micron membrane filter. Measurements of N-NO₃, P-PO₄, and N-NH₃ were conducted within 24 h from sample collection. The remaining samples were stored at 4 °C with minimum exposure to light and air until analyzed within 10 days after sampling. Prior to analysis, water samples were equilibrated to ambient temperature.

TN concentration was determined with the persulfate method, by oxidation of all nitrogenous compounds to nitrate. N-NH₃ concentrations were measured by the phenate method, and N-NO₃ and N-NO₂ concentrations were analyzed by the cadmium reduction method [31]. Organic N concentration was obtained as the difference between TN and inorganic nitrogen forms (N-NH₃, N-NO₃, and N-NO₂).

TP and TDP concentrations were determined with acid digestion, followed by the ascorbic acid method. P-PO₄ concentrations were quantified using the ascorbic acid method. Particulate phosphorus was determined as the difference between TP and TDP.

Chl_a concentration was determined according to CETESB [32]. The water samples were vacuum filtered onto a glass fiber filter and preserved frozen until quantification. The filter was macerated and steeped in 90% acetone to extract chlorophyll from the algal cells, followed by sample clarification through centrifugation. The absorbance of the clarified extract was then measured in a UV-visible spectrophotometer (Kazuaki IL-0082-BI) before and after HCl acidification.

All analysis results were quality-checked by careful standardization, procedural blank measurements, and triplicated analyses, in which samples were measured three times and averaged.

2.3. Remote Sensing Images

Chl_a in the surface water of Passaúna Reservoir was estimated from Sentinel-2 single scenes which are available every 5 days if the investigation area is cloud-free. The spatial resolution is 20 m. We used the “Case 2 Regional Coast Colour” Processor (C2RCC), which is implemented in the SNAP Toolbox [33]. The C2RCC processor provides several trained neural networks (we selected C2X) that map Sentinel-2 Level 1C data (top-of-atmosphere radiance) to (atmospherically corrected) surface reflectance and chl_a concentration.

In total, 15 images from cloud-free observations are available for the study period: 1 March 2018, 20 April 2018, 10 May 2018, 30 May 2018, 14 July 2018, 23 August 2018, 7 September 2018, 11 November 2018, 11 December 2018, 10 January 2019, 30 January 2019,

9 February 2019, and 19 February 2019. A linear regression was performed between the measured chl_a (from the time series of the continuous sensor measurement near the intake station, and from sampling stations during the campaign of 11 December 2018) and the estimated chl_a from satellite images. For the comparison with in-situ measurements, an area of 60 m × 60 m around the sampling location was averaged. To assess the longitudinal gradient of concentrations, the reservoir was divided in 10 sections of equal width of the forebay (Figure 1).

2.4. Reservoir Hydrodynamics

Reservoir hydrodynamics were assessed in previous studies in terms on the spatial variations and temporal dynamics of thermal stratification and density currents based on measurements [34] and modeling [35]. In both studies, mixed periods were defined based on Schmidt Stability (S_T) calculated from the vertical temperature profile measured at the Intake point. Therefore, the reservoir was classified as mixed when $S_T \leq 16.3 \text{ J m}^{-2}$ (10% of the annual maximum).

The applied three-dimensional hydrodynamic model was capable of reproducing stratification and large-scale flow features in Passaúna Reservoir [35]. In the present study, three sets of simulations are used: (i) The simulations of the monitoring period (February 2018 to February 2019) using present reservoir morphology, observed inflow temperature, and measured atmospheric forcing (including wind and heat fluxes); (ii) A scenario with the forebay removed, where we assessed its influence on density currents, since it is a region that can potentially disappear either due to siltation or reduced water levels during a drought period. The underlying hypothesis was that underflows were expected to become more frequent due to lower inflow temperatures, once the forebay increases surface heat exchange due to the relatively large superficial area and low water depths [34]. One of the parameters to estimate river water temperature is the percentage of stream shading in the catchment. In scenario (iii), the inflow temperature was changed according to simulations with warmer river temperature that considered the lack of stream shading (0%) in the catchment [26]. In this case, the inflow temperatures became higher and an increased occurrence of overflows was expected [26].

As an extension of the previous simulations, we assessed the distribution and dynamics of density currents along the reservoir using the simulated transport of a numerical tracer, which was added to the inflow of the Passaúna River with a constant concentration of 1 kg L⁻¹. To avoid accumulation of the tracer in the reservoir, its concentration is decreasing over time with a first-order decay rate of 0.01 d⁻¹. A dynamic classification of density currents along a longitudinal cross section of the reservoir, according to the 10 sections, was performed for the remote sensing analysis. The classification was based on the vertical tracer distribution, expressed as the tracer ratio Tr :

$$Tr = 1 - \frac{d_{MaxTr}}{d} \quad (2)$$

where d_{MaxTr} is the depth of the maximum value of the laterally averaged simulated tracer concentration, and d is the mean water depth of the respective section. Thus, values of $Tr \leq 0.33$ are defined as underflows, $Tr \geq 0.67$ as overflows, and the intermediate range as interflows.

2.5. Statistical Metrics

For the comparison of different data, statistical tests were applied: the one-way ANOVA test, which compares the variance of two groups of normally distributed data; and the Kruskal–Wallis test, which is the equivalent of ANOVA for non-parametric distributions.

Chla estimated through remote sensing images were compared to the in-situ estimations by means of root mean squared error (*RMSE*), calculated as following:

$$RMSE = \sqrt{\frac{1}{n} \sum_{i=1}^n (\hat{y}_i - y_i)^2} \quad (3)$$

where \hat{y} is the predicted value (estimation by remote sensing), y is the observed value (by in-situ sensing), and n is the number of predictions/observations. In addition, the Pearson correlation coefficient (R) was calculated.

3. Results

3.1. Continuous Observations

Air temperature had diel and seasonal variations (Figure 2a), and varied between 1.7 °C on 11 July 2018 and 33.9 °C on 29 January 2019. Wind speed was generally low, with a maximum value of 6.8 m s⁻¹ and an average \pm standard deviation of 2.0 \pm 1.0 m s⁻¹ (Figure 2b). March 2018 was a wet month regarding precipitation, which was followed by a dry period that extended until September (Figure 2b). From October on, precipitation occurred more regularly; in total, there was around 1400 mm of precipitation during the monitoring period. Regarding stratification, the reservoir is discontinuous warm polymictic, with stable thermal stratification during spring and summer, and intermittently mixing during autumn and winter (Figure 2, [34]).

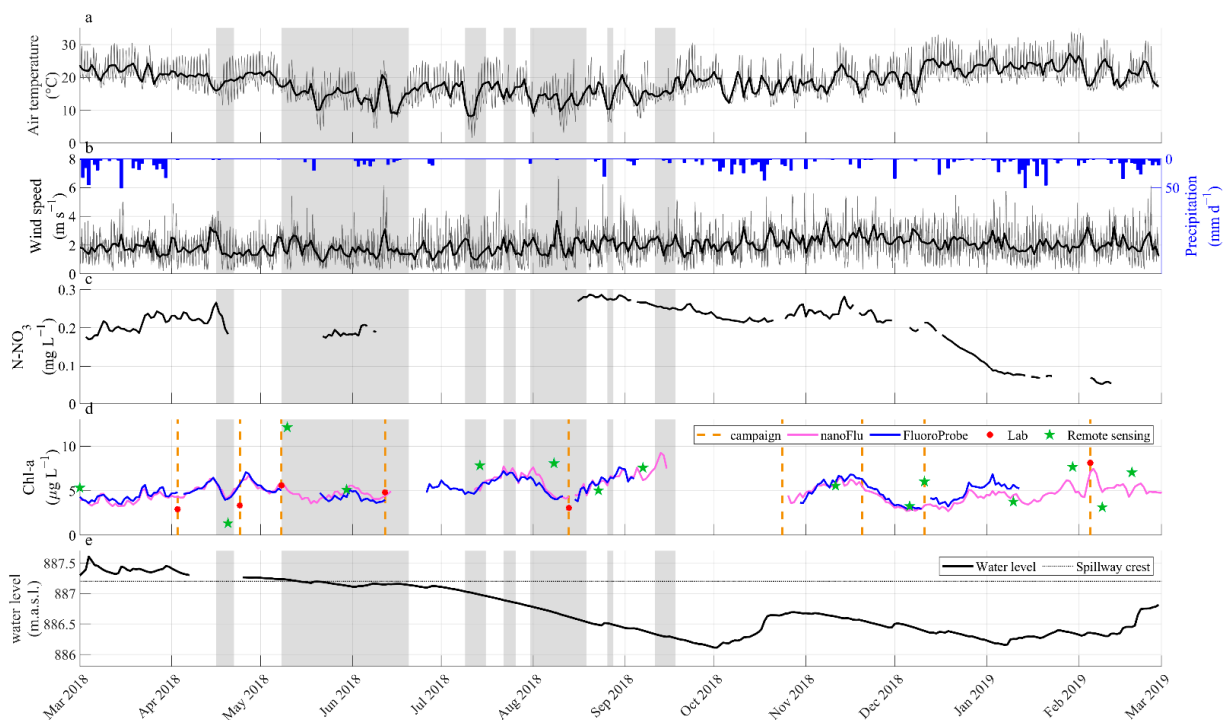


Figure 2. (a) Time series of daily mean air temperature. (b) Time series of wind speed (left y -axis, the gray fine line shows hourly averaged values and the black thick line shows daily means) and daily mean precipitation in mm d⁻¹ (right y -axis) adopted from [26,34]. (c) Time series of N-NO₃ measured by the OPUS sensor. (d) Time series of chl-a measured by sensors with daily resolution (nanoFlu (pink) and FluoroProbe (blue) solid lines), laboratorial analysis (red symbols), and remote sensing (green symbols). The dashed vertical orange lines mark the days where field campaigns were performed. Gray background color marks periods of vertical mixing in all panels; during the remaining time, the reservoir was thermally stratified (adopted from Ishikawa, Bleninger, and Lorke [34]). (e) Time series of water level in meters above sea level (m.a.s.l.) in black thick line, the dotted line shows the crest of the spillway.

Chla measured continuously at the platform location at 1.5 m depth was relatively constant throughout the year (mean \pm std: $5.2 \pm 1.5 \mu\text{g L}^{-1}$), and a marked seasonal behavior was not clear from visual inspection. However, the decrease of concentration over mixing events, followed by peaks of concentration were noted. Dividing the data in two series, concentrations over the mixed period (between the first and the last mixing event, 17 April to 17 September 2018) were significantly larger ($7.2 \pm 1.5 \mu\text{g L}^{-1}$) than during stable stratification ($5.7 \pm 1.3 \mu\text{g L}^{-1}$) according to a one-way ANOVA test (p -value $\ll 0.01$). Concentrations of N-NO₃ presented more consistent patterns over prolonged periods of time (Figure 2c). For example, the low concentrations in January and February 2019 did not affect chla concentrations, indicating that nitrogen is not a limiting nutrient in Passaúna Reservoir.

Water level fluctuations in Passaúna Reservoir were minor: over the monitored year, it varied between 886.1 and 887.6 m.a.s.l. From the middle of May, the level was constantly under the spillway crest, thus outflow at the dam occurred only through the bottom outlet.

3.2. Longitudinal Variations

Regarding the temperature stratification of the reservoir, only two campaigns were conducted during mixed periods (12 June 2018 and 13 August 2018), whereas during the remaining campaigns, the reservoir was thermally stratified (Figure 2d). Dissolved oxygen concentrations dropped to hypoxic conditions in a near-bottom layer, downstream of the Reservoir Center station, except for the two campaigns during the mixed period (Figure S3).

Nutrient concentrations (N-NO₃, N-NH₄, P-PO₄, TN, and TP) did not vary strongly between campaigns, but showed consistent longitudinal gradients along the reservoir (Figure 3). The concentrations generally decreased from higher concentrations in the inflow region to the smallest values near the dam. A particularly strong decrease was observed around station PPA (approximately 7 km from the inflow), indicating that most of the nutrients were taken up or settled before and around this location (Figure 3). Downstream of the station park (8 km from the inflow), the concentrations remained at relatively constant low levels. A different pattern was observed for N-NH₃, which remained relatively constant along the reservoir, and was strongly increased in the reservoir outflow.

Contrary to nutrient concentrations, chla was lowest in the river inflow, but increased rapidly within the reservoir, with the highest values and largest variability between the forebay and station PPA (Figure 3f). Beyond these sampling locations, chla gradually decreased towards the dam. Surprisingly, chla was comparable within the euphotic zone and below. Moreover, larger chla concentrations near the bed than at the water surface were frequently observed during the campaigns (Figure 4 and Figure S3).

During the lab analysis, it was observed that the samples collected below the euphotic zone had a brownish color, indicating that at least part of the phytoplankton was dead. The pattern of larger concentrations in deeper layers was also observed for nutrient concentrations (Figure 3).

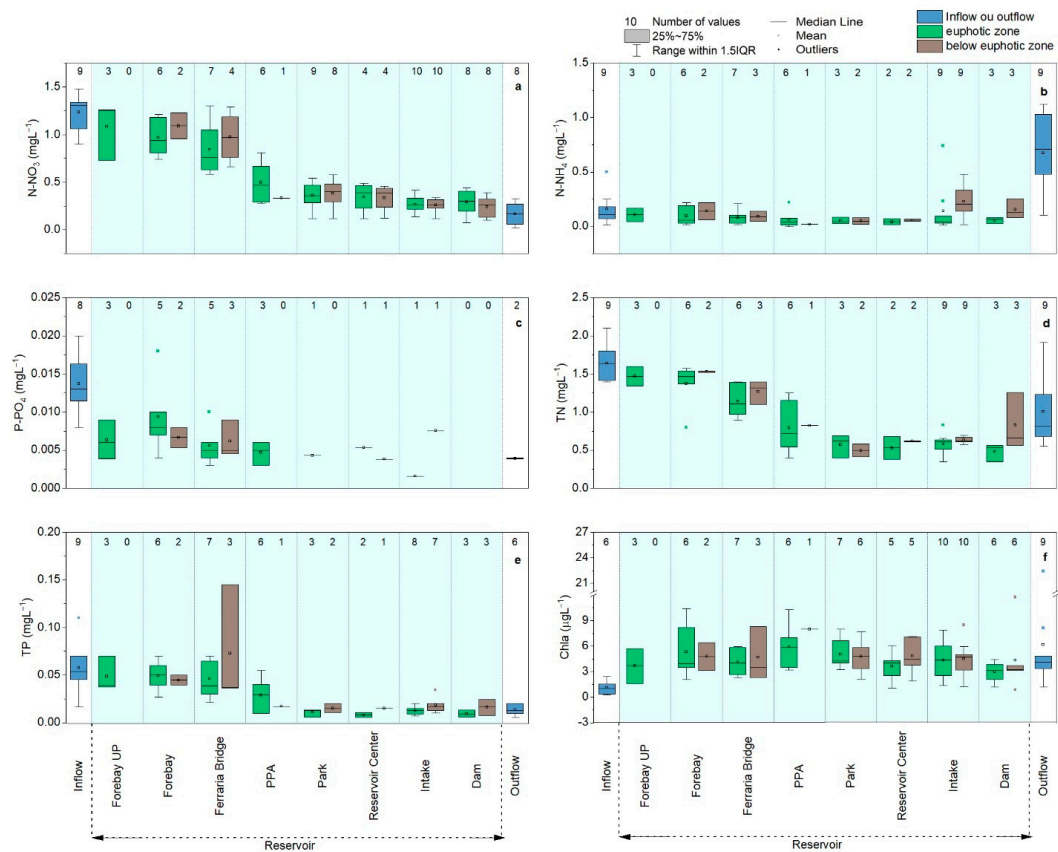


Figure 3. Box plots of water quality data estimated through laboratorial analysis and sensor measurements during all sampling campaigns at different locations along the reservoir (from inflow to outflow, see Figure 1 for the location of sampling sites). Data from different sampling sites are separated by vertical gray lines. Blue boxplots show measurements in the inflow and outflow; green boxplots show data from within the euphotic zone; and grey boxplots show data from below the euphotic zone. Numbers on the top of each boxplot represent total of samples; see the legend for an explanation of the box plot elements. Each panel presents one parameter indicated in each *y*-axis. Each panel presents the concentration of one substance: (a) N-NO₃; (b) N-NO₄; (c) P-PO₄; (d) TN; (e) TP; and (f) chla.

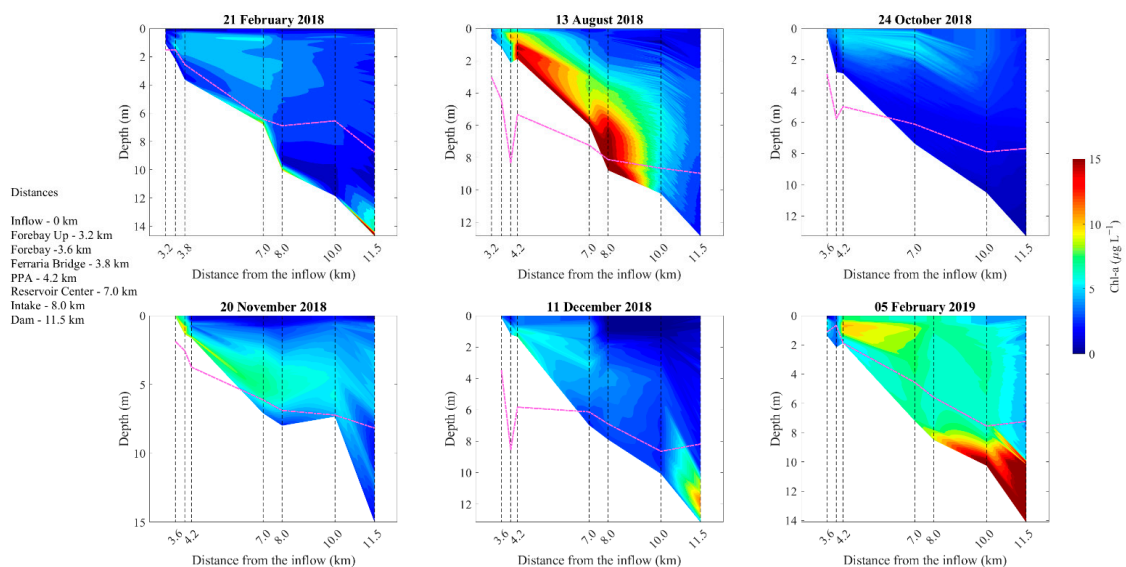


Figure 4. Contour plots of chla concentrations along a cross section of Passaúna Reservoir observed

during different sampling campaigns (the sampling date is indicated in the title of each panel). The y -axis is depth, and the x -axis is the distance along the longitudinal. The location of the sampling sites at which vertical profiles with the FluoroProbe sensor were measured is indicated by black dashed vertical lines. The profiles were interpolated along the longitudinal direction. The magenta dashed line shows the estimated depth of the euphotic zone.

3.3. Spatial Variations of Chla at the Water Surface

The three longitudinal transects had the highest concentrations between the forebay and the side arm with the Ferrara River, with the highest chla concentrations in February 2019 and the lowest in August 2018 (Figure 5).

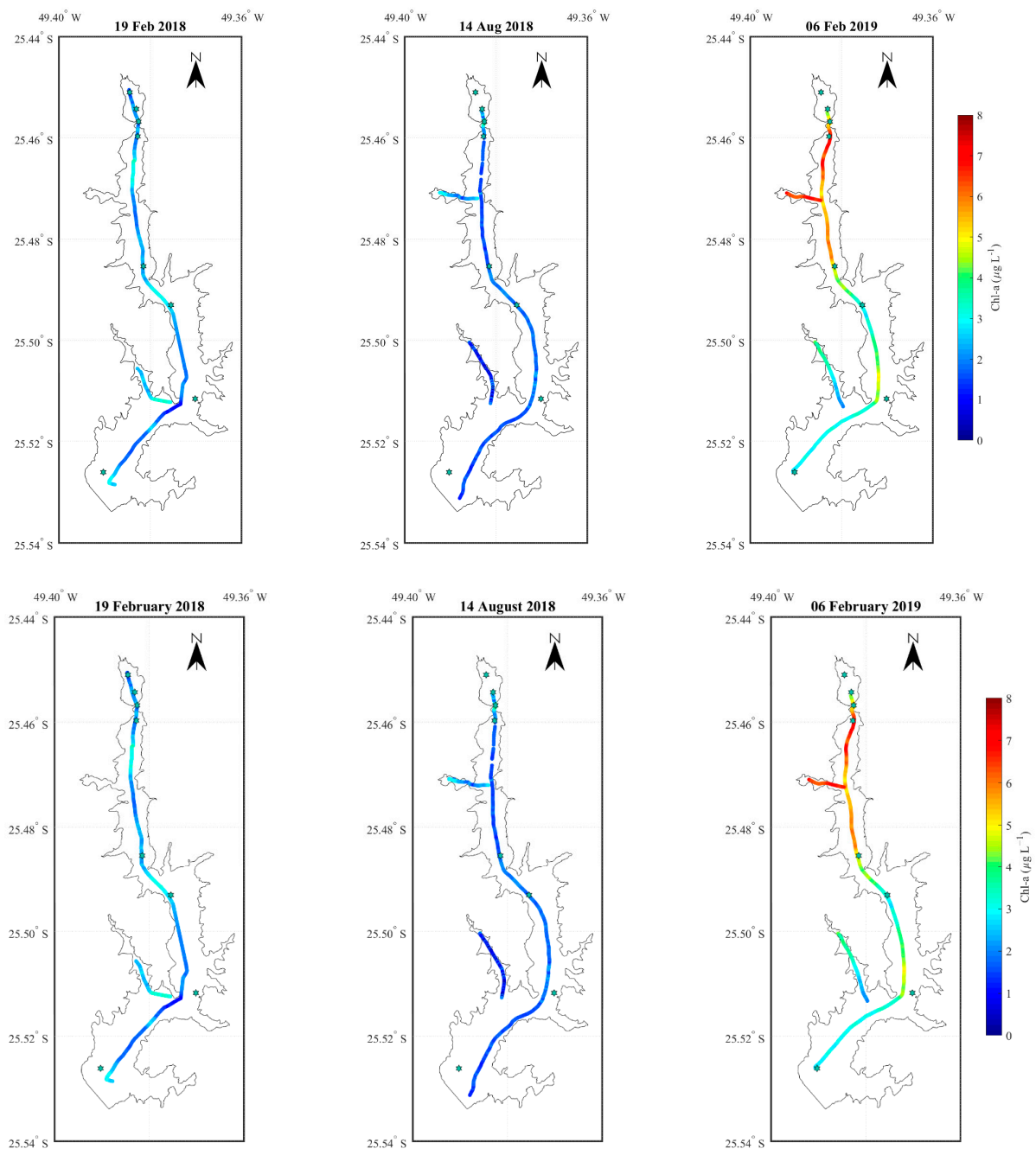


Figure 5. Longitudinal transects of chla at the water surface (~1 m depth), measured with the FluoroProbe sensor during the three extensive sampling campaigns (the sampling date indicated in the title of each panel).

Chla estimated from remote sensing images, in comparison to sensor measurements at the intake platform and the campaign in December 2018, had a root mean squared error (RMSE) of $3.7 \mu\text{g L}^{-1}$. The Pearson correlation coefficient with lab measurements was poor and not significant: $R = 0.11$ (p -value = 0.56, $n = 31$). When keeping only the data from the intake sampling location, there was a slight improvement of agreement ($\text{RMSE} = 2.8 \mu\text{g L}^{-1}$, $R = 0.32$, p -value = 0.12, $n = 24$). A systematic error was not observed through a linear regression between laboratory measurements and remote sensing estimates (Figure S4).

Despite the poor correlation, the remote sensing observations provided values in the same magnitude and longitudinal gradients similar to the observations during the in-situ measurements (Figure 6). Therefore, the dataset can support the findings of the study, especially because of the better spatial resolution at the water surface. Considering all remote sensing estimates, the mean chl-a concentration \pm standard deviation was $5.8 \pm 4.2 \mu\text{g L}^{-1}$.

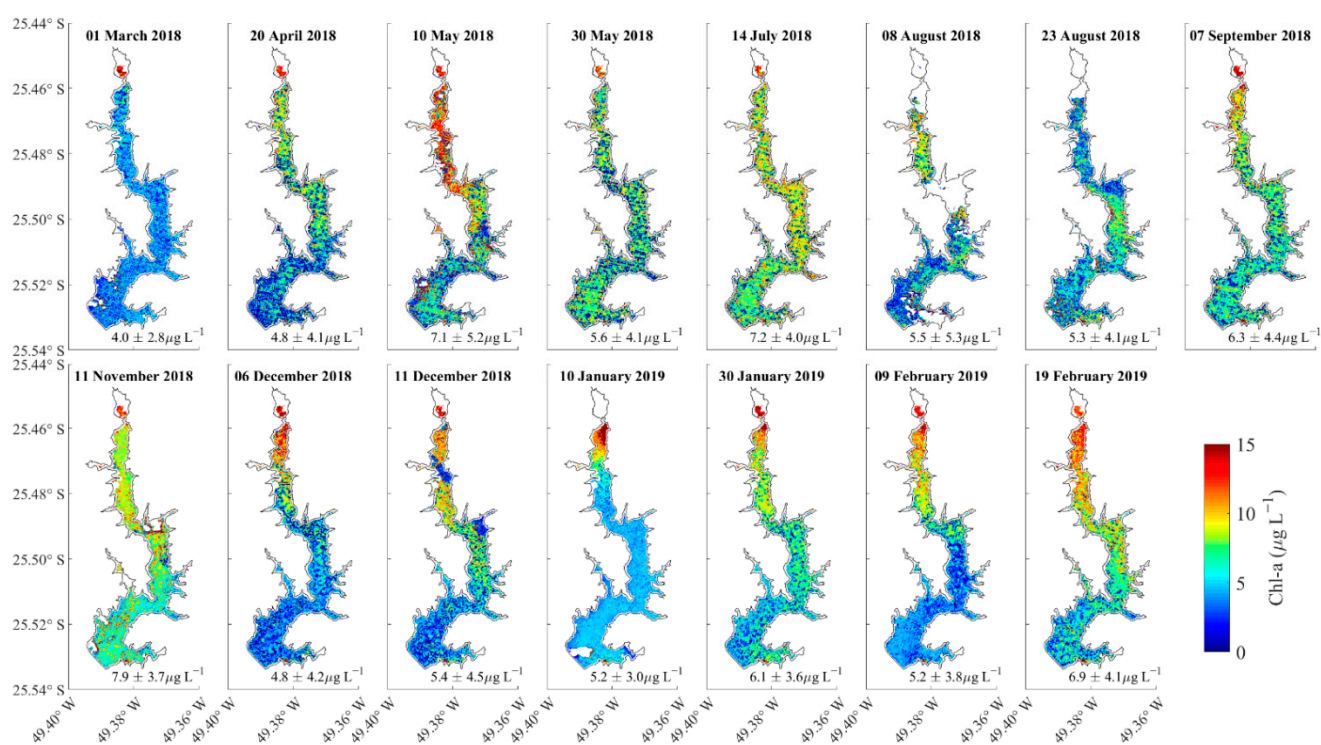


Figure 6. Maps of remote sensing estimates of chl-a concentrations for the days indicated in the title of each panel. The mean (\pm standard deviation) concentration is presented as a text label below each map.

3.4. Linking Water Quality to Physical Processes

Former analysis found seasonal variations of the density current patterns at the intake sampling station, which changed from predominantly interflows from March to mid-April 2018, to underflows during the period of frequent mixing, and to inter- and overflows starting from mid-August 2018 [35]. Here, we extended this analysis to other regions of the reservoir. The longitudinal pattern of the density current could be well followed by the simulated transport and decay of a tracer in the main inflow river (see Figure S5 for a sample distribution).

3.4.1. Temporal and Spatial Variations

In-situ sampling of the monitoring points within the euphotic zone were grouped according to the sections, since the points had variable distances among each other. In this way, the largest concentrations of chl-a were observed in section 2, (Figure 7b). The continuous surface transects (Figure 5) were also divided according to the sections, and

a similar longitudinal distribution to the samples was observed (Figure 7b). According to a Kruskal–Wallis test, none of the sections were significantly different from each other (p -value = 0.26 and 0.93, for measurements made through sampling and with the sensor, respectively).

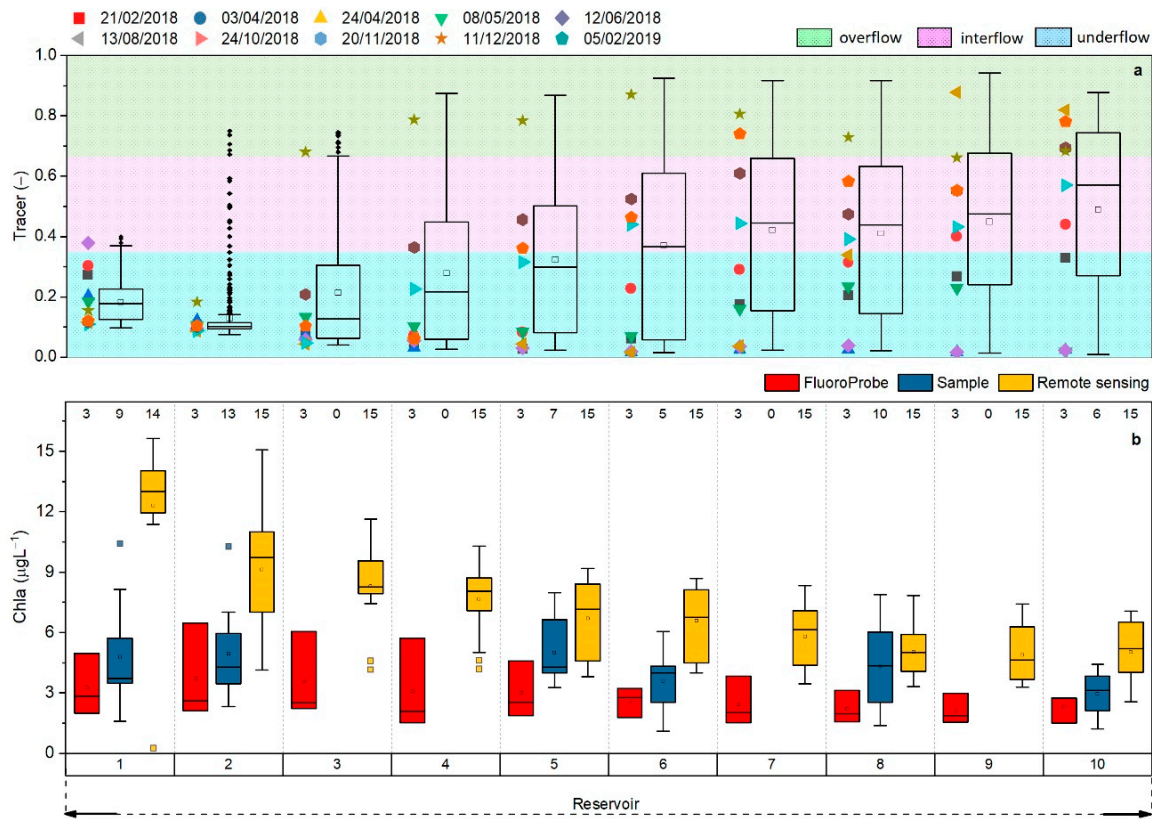


Figure 7. (a) Box plots of the temporal variations of the tracer ratio (Tr , Equation (1)) averaged for each section. The background color marks the thresholds for the three classifications of density currents (see legend). Each campaign is marked as a scatter plot. (b) Box plots showing the variability of different estimates of chl a in the 10 longitudinal zones (vertical grey lines indicate each section as divided in panel (a)). Yellow box plots represent the temporal variation of chl a from remote sensing. Blue box plots represent the temporal variation of chl a measured by analyses of water samples, for which sampling points were grouped according to sections. Red box plots represent the temporal variation of chl a measured during the three continuous longitudinal transects with the FluoroProbe sensor (Figure 5).

The longitudinal pattern of the chl a estimates from remote sensing differed from that of the in-situ measurements by showing gradually decreasing concentrations from the inflow region towards the dam (Figure 7b). The Kruskal–Wallis test showed that, in this case, chl a concentration distribution in sections 1 to 4 were significantly different from sections 8 to 10, whereas sections 5 to 7 were only significantly different from section 1 (p -value < 0.001).

The longitudinal distribution of the tracer ratio for the entire analysis period showed the smallest values in section 2 (average of 0.13), followed by a gradual increase towards the dam (Figure 7a). Underflows dominated the forebay, representing 98% of the simulated period, as well as sections 2 and 3 (96% and 76%, respectively). In sections 4 and 5, the inflow was mostly present as underflows (65% and 54%), but also inter- and overflows occurred more frequently than in the sections upstream. From section 6, the flow path was present as interflows for 34% of the period, indicating a separation of the flow paths from the bed. The occurrence of overflow situations was observed only downstream of section 4,

where its occurrence gradually increased towards the dam (at section 10, it had a share of 37%). The opposite longitudinal pattern was observed for the occurrence of underflows.

The inflow regimes during the campaigns were classified using the tracer box plots (Figure 7a). At section 1, only the campaign in 12 June 2018 was an interflow, which was at the edge of being classified as underflow. Then, in section 2, all campaigns were within underflows. The campaign in 11 December 2018 is the only one that was classified as overflow over most of the sections. The first three campaigns were consistent underflows along all sections, whereas the others shifted to interflow and eventually to overflow (e.g., 13 August 2018 and 5 February 2019). It was also possible to identify a seasonal variation in the density current pattern: underflows occur mainly during autumn and winter, and overflows during spring and summer (Figure S6).

To assess the influence of thermal stability, chl_a concentrations were analyzed separately for mixed and for conditions, based on the temperature difference between surface and bottom water. The difference was calculated from in-situ measurements, whenever they were available; otherwise, they were estimated from the model simulations (Figure 8a,b).

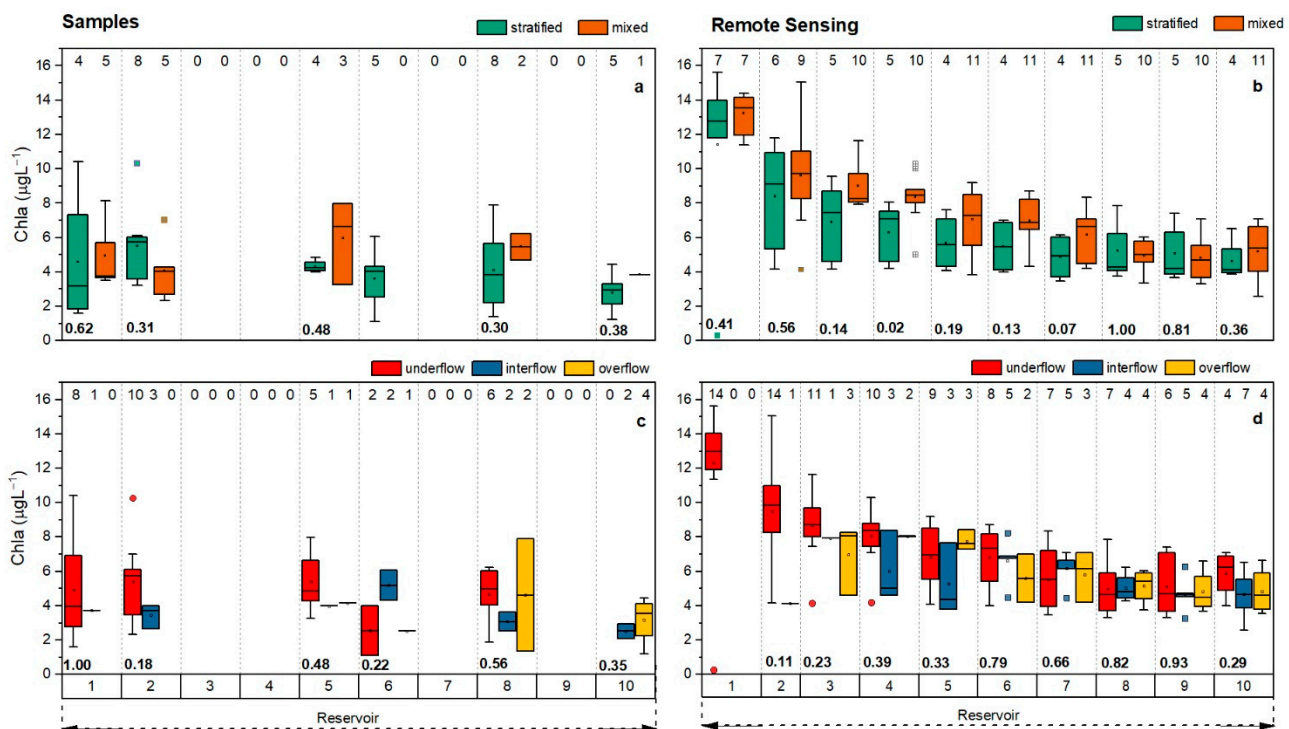


Figure 8. Box plots of chl_a concentrations observed during mixed (green) and stratified (orange) conditions from (a) laboratory analyses of water samples and (b) remote sensing estimates. Box plots of chl_a concentrations observed for different types of density currents: (c) laboratory analyses and (d) remote sensing. Each color represents one group according to the legends. Numbers at the bottom are the *p*-value of the Kruskal–Wallis test between the two groups within the section with the null hypothesis that both groups come from the same distribution.

The median values of chl_a estimated from situ data were consistently larger during mixed compared to stratified conditions, except for section 2. However, the chl_a concentration obtained from laboratory analyses of water samples did not differ significantly between mixed and stratified conditions (*p*-values > 0.05, Figure 8a), maybe due to the few and unevenly distributed samples. In addition, no consistent longitudinal trend was observed. The number of samples became more limiting when comparing chl_a measurements obtained during different types of density currents. For example, some sections had only one or no observation for some flow path groups (Figure 8c). No significant

differences between the distributions of chl_a concentrations from in-situ observations could be observed for the different types of density currents.

Contrary to the in-situ estimates, the chl_a concentrations estimated by remote sensing in the different longitudinal sections of the reservoir had consistently higher median values during stratified conditions compared to mixed conditions. However, only for section 4, the difference was significant (p -value = 0.02, Figure 8b). Only in sections 1, 8, and 9, the observed chl_a concentrations under mixed conditions had the maximum averaged observation larger than during stratified conditions. The division according to density currents did not present any systematic pattern, and all groups were similar (p -value > 0.05, Figure 8d).

We compared the original simulation of the tracer ratio to two additional scenarios (without the forebay, and without stream shading in the catchment) to understand how the changes could affect the flow paths of the density currents (Figure 9).

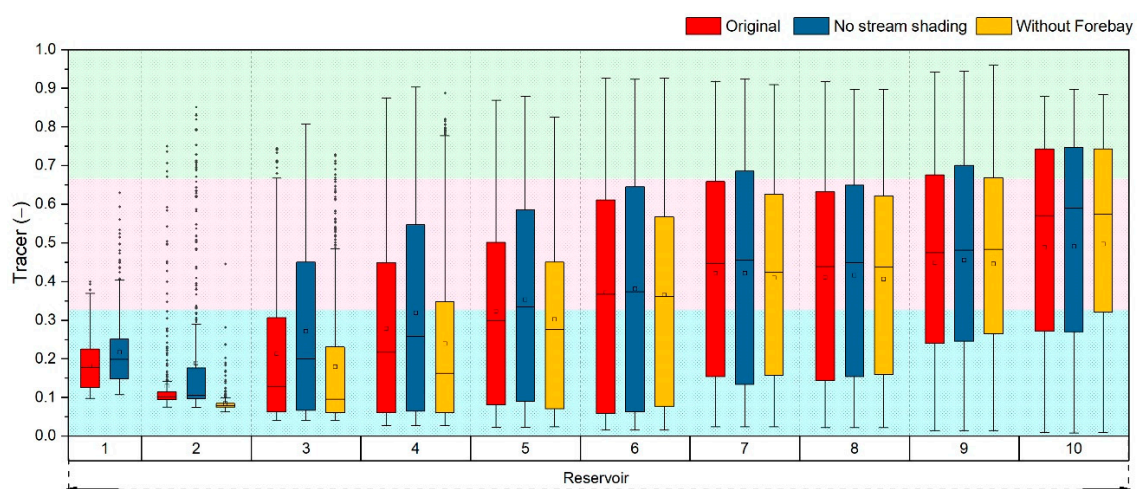


Figure 9. Box plots of tracer ratio for the original simulation and two scenarios (without the forebay and no stream shading in the catchment—indicated by the legend). Each subplot is one section, indicated by the title. The background color marks the thresholds for the three classifications of density current. Blue background represents the threshold for underflows, pink background for interflows, and green background for overflows.

The two scenarios presented the expected variations for density currents, but the changes were generally small. The most pronounced shift happened at section 2, which is right after the forebay, where, in the original simulation, underflows represented 95% of the density currents, it increased to 99% without the forebay, and decreased to 86% without stream shading. Similar differences were observed until section 4, whereas in more downstream sections, the distributions were unaffected, indicating that, from section 6, the influence of the inflow temperature was of minor relevance.

3.4.2. Correlations

For each of the 10 longitudinal sections of the reservoir, we calculated Pearson correlation coefficients between chl_a estimated from in-situ measurements and from remote sensing with the following parameters: inflow concentration of TP, P-PO₄, TN, N-NO₃, N-NH₄ (interpolated to a daily resolution from the in-situ measurements); Schmidt stability (S_T); average temperature difference between surface and bottom at each section (ΔT , model results); inflow temperature; and tracer ratio (T_r) (Figure 10). The sampled chl_a within the euphotic zone was correlated only with the temperature difference ΔT in section 2 (positive correlation). Remote sensing estimates of chl_a were positively correlated with Schmidt stability, ΔT , and inflow temperature in sections 1 and 2. Section 2 also had a positive correlation with P-PO₄, and a negative correlation with N-NO₃. From sections

by internal loading with nutrients [39,40]. This is further supported by higher nutrient concentrations in deeper layers than near the water surface (Figure 3). In addition, averaged chl_a concentrations were larger over the periods where the mixing events occurred: during the autumn and winter seasons.

There are indications of N limitation in tropical lakes [41]; however, the continuous measurements at the monitoring platform at the intake suggested that the large variations of the N-NO₃ did not affect the chl_a dynamics, indicating that the N limitation was not relevant. In addition, the P limitation at Passaúna Reservoir was observed through the assessment of the annual average of inflow concentrations of TP and TN according to the scheme presented by Sterner [42].

The observed longitudinal decrease of nutrients (TN and TP) in Passaúna Reservoir (Figure 3) supports the conceptual model of [20] and observations in other reservoirs (e.g., [43,44]). The observed chl_a concentrations were in accordance with the proposed framework, showing the largest concentrations in a region between the riverine and lacustrine zones. This was more evident when grouping the sampled data in sections of equal distance (Figure 7b). When evaluating each point individually, chl_a concentrations had their largest values at the forebay and PPA. Between these two sampling locations, there was Ferraria Bridge, where concentrations were lower at the water surface than in deeper layers. At this point, the reservoir is laterally constrained to a channel-like region (see Figure 1), which may have influenced the vertical distribution (Figure 3). When grouping the data in sections, the second section presented the largest concentrations of chl_a, and a similar pattern was observed in the continuous longitudinal sensor transect (Figure 5). However, the concentration distributions of the different sections were not significantly different among each other. TP and TN had lower concentrations in the outflow from the reservoir compared to the inflow, indicating the trapping of nutrients by the dam. This was observed for all chemical nutrient speciation, except for N-NH₄, which had the largest concentrations at the outflow, a feature caused by the anoxic conditions found at the deepest layers close to the dam. Hence, most of the outflow was from the bottom outlet (all during the period when the water level was lower than the spillway crest—Figure 2e), and outflow concentrations were similar to the ones found in the deepest regions around the dam. On the other hand, chl_a had larger concentrations at the outflow than at the inflow.

The distinct longitudinal distribution of chl_a in reservoirs has not been observed in all studies, with many examples in which the largest concentration of chl_a was observed at the riverine zone [43–45], and at the lacustrine zone due to the mobilization of nutrients from the sediment [45]. A quantitative criterion for the definition or the prediction of the reservoir sections belonging to the riverine, transitional, and lacustrine zones is not trivial. Their location depends on morphological characteristics, flow velocities, light availability, and nutrient levels. Moreover, these zones can expand and compress over time [46]. Whereas other studies defined those regions through data clustering of the aforementioned parameters [37,47], we tried to do the same analysis, but the results were inconsistent. We believe that the main causes are the uneven distribution of sampling points along the longitudinal, and the missing measurements upstream between April and June (Table S1). A classification based on model results was also attempted; in this case, the variables used were morphological (depth and width) and flow velocities. For this reason, we evaluated the gradients according to the longitudinal distribution of nutrients and chl_a, which is more relevant than defined zones. In addition, for reservoirs with a dendritic shape, or with more than one relevant inflow, the zonation can become less meaningful.

In contrast to the in-situ measurements, chl_a estimated by remote sensing had its largest concentrations in the most upstream regions, and it decreased continuously until the dam. The greatest differences between remote sensing and in-situ chl_a estimates occurred in section 1, and the difference was gradually decreasing along the reservoir. However, the remote-sensing-based estimates had a root mean square error of $\pm 3.7 \mu\text{g L}^{-1}$, which is smaller than the expected error for chl_a estimations from the Sentinel-2 observation of $5\text{--}10 \mu\text{g L}^{-1}$ [48,49]. Thus, for the low range of chl_a values in Passaúna Reservoir from

the in-situ reference (mostly between 4 and 7 $\mu\text{g L}^{-1}$, see Figure 2c), a strong correlation between observed and estimated chl_a variations over time cannot be expected. Yet, spatial patterns observed in individual remote sensing scenes may be meaningful, in that it may be a systematic error per scene. The comparison of remote-sensing-based and in-situ measurements time series suggests that the remote-sensing-based method is sensitive to small temporal changes. There are several sources contributing to the disagreement of in-situ and remote-sensing-based values, such as the mismatch of the field of view of in-situ and remote optical sensors, temporal mismatch, remote sensing model error, and in-situ sensor error (disagreement between sensor and lab analysis). However, we cannot estimate the individual contribution of each error source.

In laboratory analyses, although the samples were kept in the dark for their preservation, they were filtered several hours after sample collection (when they arrived in the laboratory). Further, chlorophyll was extracted from the samples by manual maceration. Each step is susceptible to add uncertainties. On the other hand, sensor measurements have the advantage of taking measurements in-situ, but can be affected by the sunlight, and present a limitation on the measurement range depending on the optical path. As the laboratorial analysis is a well-established method, we usually take its result as the reference for the comparison with sensor and remote-sensing-based estimates.

4.2. Effects of Density Currents

The results from the numerical model showed good agreement with observed temperatures ($RMSE = 0.77\text{ }^{\circ}\text{C}$) [35], and for Passaúna Reservoir, the main driver of changes in inflow density is temperature [34]. Thus, the simulated tracer transport is considered a good approach for evaluating the flow paths of density currents. This is supported by previous studies using numerical tracers as a proxy for density currents, which showed good agreement with in-situ observations of dye tracers [50].

The sampling campaigns on 13 August 2018 and on 5 February 2019 were conducted for similar nutrient concentrations in the reservoir inflow ($\text{TN} = 1.5$ and 1.6 mg L^{-1} , $\text{TP} = 0.04$ and 0.05 mg L^{-1}), yet the longitudinal transects showed that chl_a at the water surface was about a factor of two lower in August than in February (Figure 5). Based on the tracer ratio analysis from the numerical model (Figure 9), the campaign in August was dominated by an underflow (except in the two last sections), and the other campaign varied from underflow in sections 1 to 4, and to inter- and overflow in the rest of the reservoir. In addition, sensor profiling (Figure 4) showed that the highest concentrations of chl_a in August were in the deeper layers. This indicates that nutrients were consumed in the upstream region, where the euphotic zone encompassed the entire water column, and the algae were transported by the density current to larger depths. When dividing the sampled data set in groups of under-, inter-, and overflow (Figure 8c), chl_a had the largest concentrations in interflows (section 6) and overflows (sections 8 and 10). However, the groups were statistically similar, which agrees with the generally small temporal variability of chl_a.

Density currents varied seasonally (Figure S6), and it was expected that they could promote seasonal variations in chl_a [24,35]; however, this was not observed. One explanation for not seeing a significant difference according to the flow path over time is related to water depth in relation to the euphotic zone. Until section 4 (maximum water depth $\sim 7\text{ m}$), the estimated depth of the euphotic zone was larger than the water depth on some occasions. Therefore, even when nutrients were delivered directly to the bottom, they were within the euphotic zone available for algal growth. Because of the shallower depths, the region mixed more frequently than downstream regions, making the surface concentrations of chl_a independent of the density current pattern. Since inflow concentrations were rather constant, temporal variations were minor.

Regarding the simulated scenarios, simulation without the forebay increased the formation of underflows significantly until section 3 (p -values < 0.001). The other scenario, with higher inflow temperatures due to the removal of stream shading in the catchment,

increased the formation of overflows until section 4 (p -values ≤ 0.03). In both simulations, the density currents were not influenced by the inflow conditions downstream of this section. In that regard, our simulations confirm previous analyses of the expected changes of density currents in both scenarios [26,34]. In these studies, density currents were classified based on inflow temperature and on the vertical temperature profile measured at the intake (section 8), which excluded vertical mixing during transport along the longitudinal extent of the reservoir. Indeed, there was the increase of under- or overflows depending on the scenario; however, these changes could not be seen at the intake. According to the model, the shift is only seen until the park station. The inflowing water can be mixed vertically before it is transported longitudinally to regions with water depths exceeding that of the surface mixed layer. In this way, it is possible that the currents classified as interflows or underflows move forward along the water surface. This was observed in the tracer simulations, and due to the small water depth until section 5, it was common to have a vertical mixing over the entire water column during the entire year.

Sotiri, et al. [51] assessed the sediment thickness of Passaúna Reservoir, and identified two major zones of sedimentation, which correspond to sections 2 and 9 of this study. The first region upstream is linked to sedimentation from inflow, where we found most algal growth. Our observations show that the second sedimentation zone, closer to the dam, is likely formed by the enhanced deposition of algae that are transported there from the inflow region by density currents. This is supported by the assessment of organic matter content in the sediment presented in Marcon, et al. [52], where at section 2, organic matter was $<10\%$ of the sediment content, and in the downstream regions, it was $>30\%$. Enhanced deposition of autochthonous organic matter explains the persistent formation of anoxic conditions of the deeper layers in the downstream region of the reservoir, as they were observed in most campaigns (Figure S3) and in previously analyzed continuous oxygen measurements performed near the intake station [34]. Using the sediment surface area and reservoir water volume for water depth exceeding 9 m, the areal hypolimnetic oxygen deficit (AHOD, Hutchinson [53]) calculated from the temporal rate of decrease of dissolved oxygen concentration in the hypolimnion observed in [34] was approximately $1.0 \text{ g of O}_2 \text{ m}^{-2} \text{ day}^{-1}$. The AHOD observed in Passaúna is in the same range as eutrophic lakes in the temperate zone [54], though Passaúna is classified as mesotrophic. Moreover, the two regions with high sedimentation rates are characterized by the highest emissions and production rates of methane [52].

4.3. Correlations between Nutrient and Chlorophyll Concentrations

With an annual mean inflow concentration of total phosphorous (TP) of 0.06 mg L^{-1} , the averaged concentration of chl_a measured in-situ (at all depths and all campaigns) of $4.4 \text{ } \mu\text{g L}^{-1}$ in Passaúna Reservoir is in the lower range of values predicted by linear models between both variables that have been established for different lakes and reservoirs, and range between 5.0 and $30.2 \text{ } \mu\text{g L}^{-1}$ (Table S2). The relationship that provided the closest result to the observations was the one presented by Stow and Cha [7], though its relationship was found for Lake Huron; nevertheless, other results were within the error margin.

Correlations between spatial and temporal variations of chl_a and TP in Passaúna Reservoir were generally poor, and the same was observed for correlation with other parameters. Carneiro, et al. [55], and Klippel, Macêdo, and Branco [1] also found poor results for direct relationships between total phosphorus and chl_a in Brazilian reservoirs. They considered data for periods of one month and three years, respectively. Cunha, Finkler, Lamparelli, Calijuri, Dodds, and Carlson [2] found better linear relationships between TP and chl_a using annual mean values from six reservoirs in Brazil for a period of nine years. An increase in sample number by merging the in-situ and remote sensing data did not improve the correlations. Nevertheless, remote-sensing-based chl_a estimates had the largest difference in regard to longitudinal pattern in the two first sections when compared to in-situ measurements, which can put the results from these zones into question. For sections

where there was not much difference between the two datasets (e.g., section 6), Schmidt stability had negative correlations, which agrees with the observation of declining chl_a concentrations during mixing, and higher values during restratification periods (Figure 2c). In the data from continuous measurements of chl_a and Schmidt stability, the correlation between both parameters was poor, most likely because the trigger for the increased algal growth is the mixing event, i.e., change of the strength of stratification.

From the poor correlations between observed chl_a variability and environmental conditions, we comprehend that the processes that are controlling phytoplankton dynamics are more complex than linear relationships, and additional processes should be considered when assessing results at different spatial and temporal scales. For example, during the campaign in October 2018, the total phosphorus concentration in Passaúna River was highest; however, the chl_a concentrations in the reservoir were the smallest. This counterintuitive observation can potentially be explained by a rain event that occurred in this month, which mobilized nutrients, increased the flow rates, and reduced the residence time, which are not favorable for phytoplankton growth [56]. Another feature was the concentration maximum of chl_a at deeper, near-bed layers, where the concentration frequently exceeded those measured near the water surface. Our analysis suggests that they were transported by density currents from upstream regions. Depending on the mixing condition, type of density current, and euphotic zone depth, concentrations of chl_a can be highest at the water surface, even in the presence of underflows.

5. Conclusions

The use of fast in-situ probes on a moving boat, combined with remote sensing techniques and 3D hydrodynamic modeling allowed us to map and link water quality and hydrodynamic features in a drinking water reservoir located in the subtropical zone. Despite the seasonal variation of density currents and thermal stratification, the chlorophyll-*a* concentration (chl_a) did not follow a seasonal pattern (standard deviation of 1.2 $\mu\text{g L}^{-1}$, at the continuous measurement station), whereas spatial variability was more pronounced (standard deviation of 2.1 $\mu\text{g L}^{-1}$, among all monitored points within the euphotic zone). The small temporal variability was caused by the shallow depth of water in the productive upstream region of the reservoir, where the entire water column was within the euphotic zone and was frequently mixed throughout the year. Thus, even with the delivery of nutrients to deeper layers by inflowing river water as underflows, they were available for the growth of phytoplankton. The algae grown in the upstream region of the reservoir were transported downstream by the density currents, resulting in the highest concentrations of chl_a below the euphotic zone at larger water depths. Most nutrients were consumed in the upstream region, and primary production in the lacustrine zone depended on internal loading, and was promoted by mixing events.

Linear correlations between temporal variations of the concentration of chl_a and total phosphorus (TP), thermal stability, and density current patterns at specific points in the reservoir were generally poor. On the other hand, the annual mean values of chl_a and TP were in the lower range of linear models relating both parameters across different lakes and reservoirs. Such relationships can inform about seasonal and basin-scale mean chl_a concentrations, but fail in reproducing its spatial and temporal dynamics, for which the distribution and dynamics of both nutrients and algae are strongly influenced by hydrodynamic processes.

We expect that the dynamics of nutrient delivery and phytoplankton transport by density currents observed in Passaúna Reservoir are representative of a large number of reservoirs. For deeper reservoirs, where the euphotic zone is restricted to a smaller longitudinal extent, or flow velocities are larger (pushing the transitional zone towards larger water depth), more pronounced seasonal variations of chl_a could be induced by variations of density currents. Under such conditions, the simulated scenarios with increasing occurrence of overflow situations in the upstream reservoir region could increase the primary production of the system. For Passaúna Reservoir, a significant increase of nutrient

concentration in the inflow would probably be required to compromise its water quality, if nutrients would not be consumed completely in the upstream region and became available also for the lacustrine regions. However, our analyses suggest that phytoplankton growth in the lacustrine zone of the reservoir is controlled by internal loading. Internal loading can increase over time due to the increasing accumulation of phosphorus in the sediment, and due to higher temperatures that increase organic matter decomposition rates, and cause more persistent water column stratification with anoxic conditions in the hypolimnion. Additionally, drought periods with lower water levels and intensified near-bed mixing can increase internal loading episodically. Therefore, internal loading can become a trigger for degradation of water quality in the lacustrine region.

For spatial variations within the reservoir and temporal variability of chlorophyll dynamics, linear statistical models were not sufficient to provide predictions. These features can potentially be resolved by applying coupled hydrodynamic and water quality models. The persistent longitudinal gradients and the importance of density currents for the transport and distribution of nutrients, algae, and detritus revealed in our analyses suggest that at least two dimensions (depth and longitudinal) should be considered in hydrodynamic and water quality models for reservoirs.

Supplementary Materials: The following supporting information can be downloaded at: <https://www.mdpi.com/article/10.3390/w14101544/s1>, Figures S1–S6; Tables S1 and S2.

Author Contributions: Conceptualization, M.I., A.L., L.G. and T.B.; field campaigns, M.I., L.G., H.R. and T.B.; laboratorial analysis, L.G.; validation of sensor's data, H.R., L.G. and M.I.; formal analysis, M.I. and L.G.; remote sensing images acquisition, processing, and validation, N.W.; writing—original draft preparation, M.I. and L.G.; writing—review and editing, A.L., T.B., N.W. and H.R.; supervision, A.L. and T.B. All authors have read and agreed to the published version of the manuscript.

Funding: This research was funded by the Federal Ministry of Education and Research by the MuDak-WRM project under the grant numbers: 02WGR1431B, 02WGR1431G, and 02WGR1431E. In addition, Bleninger acknowledges the productivity stipend from the National Council for Scientific and Technological Development—CNPq, grant no. 312211/2020-1, call 09/2020. This study was financed in part by the Coordenação de Aperfeiçoamento de Pessoal de Nível Superior—Brasil (CAPES)—Finance Code 001. Luziadne Gurski acknowledges CAPES for financial support and Ph.D. scholarship.

Data Availability Statement: The data that support the findings of this study are available upon request from the authors.

Acknowledgments: The authors are thankful for all of the team involved in the campaign planning, execution, platform maintenance, and sample analysis, which include people from MuDak-WRM project, the Sanitation Company of Paraná (SANEPAR), and the Graduate Program of Water Resources and Environmental Engineer of Federal University of Paraná, especially Heloise Knapik and Luciane Prado.

Conflicts of Interest: The authors declare no conflict of interest.

References

1. Klippel, G.; Macêdo, R.L.; Branco, C.W.C. Comparison of different trophic state indices applied to tropical reservoirs. *Lakes Reserv. Sci. Policy Manag. Sustain. Use* **2020**, *25*, 214–229. [[CrossRef](#)]
2. Cunha, D.G.F.; Finkler, N.R.; Lamparelli, M.C.; Calijuri, M.d.C.; Dodds, W.K.; Carlson, R.E. Characterizing Trophic State in Tropical/Subtropical Reservoirs: Deviations among Indexes in the Lower Latitudes. *Environ. Manag.* **2021**, *68*, 491–504. [[CrossRef](#)]
3. Megard, R.O. Phytoplankton, Photosynthesis, And Phosphorus In Lake Minnetonka, Minnesota1. *Limnol. Oceanogr.* **1972**, *17*, 68–87. [[CrossRef](#)]
4. Havens, K.E.; Nürnberg, G.K. The Phosphorus-Chlorophyll Relationship in Lakes: Potential Influences of Color and Mixing Regime. *Lake Reserv. Manag.* **2004**, *20*, 188–196. [[CrossRef](#)]
5. Dillon, P.J.; Rigler, F.H. The phosphorus-chlorophyll relationship in lakes1,2. *Limnol. Oceanogr.* **1974**, *19*, 767–773. [[CrossRef](#)]
6. Phillips, G.; Pietiläinen, O.P.; Carvalho, L.; Solimini, A.; Lyche Solheim, A.; Cardoso, A.C. Chlorophyll–nutrient relationships of different lake types using a large European dataset. *Aquat. Ecol.* **2008**, *42*, 213–226. [[CrossRef](#)]

7. Stow, C.A.; Cha, Y. Are Chlorophyll a–Total Phosphorus Correlations Useful for Inference and Prediction? *Environ. Sci. Technol.* **2013**, *47*, 3768–3773. [[CrossRef](#)]
8. Quinlan, R.; Filazzola, A.; Mahdiyan, O.; Shuvo, A.; Blagrove, K.; Ewins, C.; Moslenko, L.; Gray, D.K.; O'Reilly, C.M.; Sharma, S. Relationships of total phosphorus and chlorophyll in lakes worldwide. *Limnol. Oceanogr.* **2021**, *66*, 392–404. [[CrossRef](#)]
9. Abell, J.M.; Özkundakci, D.; Hamilton, D.P.; Jones, J.R. Latitudinal variation in nutrient stoichiometry and chlorophyll–nutrient relationships in lakes: A global study. *Fundam. Appl. Limnol.* **2012**, *181*, 1–14. [[CrossRef](#)]
10. Filstrup, C.T.; Wagner, T.; Soranno, P.A.; Stanley, E.H.; Stow, C.A.; Webster, K.E.; Downing, J.A. Regional variability among nonlinear chlorophyll–phosphorus relationships in lakes. *Limnol. Oceanogr.* **2014**, *59*, 1691–1703. [[CrossRef](#)]
11. Shuvo, A.; O'Reilly, C.M.; Blagrove, K.; Ewins, C.; Filazzola, A.; Gray, D.; Mahdiyan, O.; Moslenko, L.; Quinlan, R.; Sharma, S. Total phosphorus and climate are equally important predictors of water quality in lakes. *Aquat. Sci.* **2021**, *83*, 16. [[CrossRef](#)]
12. Lewis, W.M., Jr. Tropical lakes: How latitude makes a difference. In *Perspectives in Tropical Limnology*; SPB Academic Publishing: Amsterdam, The Netherlands, 1996; Volume 4364.
13. Winton, R.S.; Calamita, E.; Wehrli, B. Reviews and syntheses: Dams, water quality and tropical reservoir stratification. *Biogeosciences* **2019**, *16*, 1657–1671. [[CrossRef](#)]
14. Mulligan, M.; van Soesbergen, A.; Sáenz, L. GOODD, a global dataset of more than 38,000 georeferenced dams. *Sci. Data* **2020**, *7*, 31. [[CrossRef](#)]
15. Zarfl, C.; Lumsdon, A.E.; Berlekamp, J.; Tydecks, L.; Tockner, K. A global boom in hydropower dam construction. *Aquat. Sci.* **2014**, *77*, 161–170. [[CrossRef](#)]
16. Yasarer, L.M.W.; Sturm, B.S.M. Potential impacts of climate change on reservoir services and management approaches. *Lake Reserv. Manag.* **2016**, *32*, 13–26. [[CrossRef](#)]
17. Fadel, A.; Sharaf, N.; Siblini, M.; Slim, K.; Kobaiissi, A. A simple modelling approach to simulate the effect of different climate scenarios on toxic cyanobacterial bloom in a eutrophic reservoir. *Ecolhydrol. Hydrobiol.* **2019**, *19*, 359–369. [[CrossRef](#)]
18. Weber, C.J.; Weihrauch, C. Autogenous Eutrophication, Anthropogenic Eutrophication, and Climate Change: Insights from the Antrift Reservoir (Hesse, Germany). *Soil Syst.* **2020**, *4*, 29. [[CrossRef](#)]
19. Kimmel, B.L.; Lind, O.T.; Paulson, L.J. Reservoir primary productivity. In *Reservoir Limnology: Ecological Perspectives*; John Wiley & Sons, Inc.: Hoboken, NJ, USA, 1990; Volume 1, pp. 133–199.
20. Kimmel, B.L.; Groeger, A.W. Factors Controlling Primary Production In Lakes And Reservoirs: A Perspective. *Lake Reserv. Manag.* **1984**, *1*, 277–281. [[CrossRef](#)]
21. Noori, R.; Ansari, E.; Jeong, Y.-W.; Aradpour, S.; Maghrebi, M.; Hosseinzadeh, M.; Bateni, S.M. Hyper-Nutrient Enrichment Status in the Sabalan Lake, Iran. *Water* **2021**, *13*, 2874. [[CrossRef](#)]
22. Sun, H.; Lu, X.; Yu, R.; Yang, J.; Liu, X.; Cao, Z.; Zhang, Z.; Li, M.; Geng, Y. Eutrophication decreased CO₂ but increased CH₄ emissions from lake: A case study of a shallow Lake Ulansuhai. *Water Res.* **2021**, *201*, 117363. [[CrossRef](#)]
23. Gholizadeh, M.H.; Melesse, A.M.; Reddi, L. A Comprehensive Review on Water Quality Parameters Estimation Using Remote Sensing Techniques. *Sensors* **2016**, *16*, 1298. [[CrossRef](#)] [[PubMed](#)]
24. Rueda, F.J.; Fleenor, W.E.; de Vicente, I. Pathways of river nutrients towards the euphotic zone in a deep-reservoir of small size: Uncertainty analysis. *Ecol. Model.* **2007**, *202*, 345–361. [[CrossRef](#)]
25. Cortés, A.; Fleenor, W.; Wells, M.; de Vicente, I.; Rueda, F. Pathways of river water to the surface layers of stratified reservoirs. *Limnol. Oceanogr.* **2014**, *59*, 233–250. [[CrossRef](#)]
26. Ishikawa, M.; Haag, I.; Krumm, J.; Teltscher, K.; Lorke, A. The effect of stream shading on the inflow characteristics in a downstream reservoir. *River Res. Appl.* **2021**, *37*, 943–954. [[CrossRef](#)]
27. Sanepar, C.d.S.d.P. Plano Diretor SAIC: Sistema de Abastecimento de Água Integrado de Curitiba e Região Metropolitana. *Curitiba Sanepar* **2013**. Available online: <https://site.sanepar.com.br/arquivos/saicplanodiretor.pdf> (accessed on 30 September 2020).
28. Sotiri, K.; Hilgert, S.; Fuchs, S. Sediment classification in a Brazilian reservoir: Pros and cons of parametric low frequencies. *Adv. Oceanogr. Limnol.* **2019**, *10*. [[CrossRef](#)]
29. Luhtala, H.; Tolvanen, H. Optimizing the Use of Secchi Depth as a Proxy for Euphotic Depth in Coastal Waters: An Empirical Study from the Baltic Sea. *ISPRS Int. J. Geo-Inf.* **2013**, *2*, 1153–1168. [[CrossRef](#)]
30. Rouso, B.Z.; Bertone, E.; Stewart, R.A.; Rinke, K.; Hamilton, D.P. Light-induced fluorescence quenching leads to errors in sensor measurements of phytoplankton chlorophyll and phycocyanin. *Water Res.* **2021**, *198*, 117133. [[CrossRef](#)]
31. APHA. *Standard Methods for the Examination of Water and Wastewater*, 21st ed.; American Public Health Association: Washington, DC, USA, 2005.
32. COMPANHIA AMBIENTAL DO ESTADO DE SÃO PAULO (CETESB). *L5.306: Determinação de Clorofila a e Feofitina a: Método Espectrofotométrico*, 3rd ed.; Companhia Ambiental do Estado de São Paulo: São Paulo, Brazil, 2014.
33. Brockmann, C.; Doerffer, R.; Peters, M.; Kerstin, S.; Embacher, S.; Ruescas, A. Evolution of the C2RCC Neural Network for Sentinel 2 and 3 for the Retrieval of Ocean Colour Products in Normal and Extreme Optically Complex Waters. In Proceedings of the conference: Living Planet Symposium 2016, Prague, Czech Republic, 1 August 2016; p. 54.
34. Ishikawa, M.; Bleninger, T.; Lorke, A. Hydrodynamics and mixing mechanisms in a subtropical reservoir. *Inland Waters* **2021**, *11*, 286–301. [[CrossRef](#)]
35. Ishikawa, M.; Gonzalez, W.; Golyjeswski, O.; Sales, G.; Rigotti, J.A.; Bleninger, T.; Mannich, M.; Lorke, A. Effects of dimensionality on the performance of hydrodynamic models for stratified lakes and reservoirs. *Geosci. Model Dev.* **2022**, *15*, 2197–2220. [[CrossRef](#)]

36. Wetzel, R.G. *Limnology: Lake and River Ecosystems*; Academic Press: San Diego, CA, USA; London, UK, 2001.
37. de Oliveira, T.F.; de Sousa Brandão, I.L.; Mannaerts, C.M.; Hauser-Davis, R.A.; Ferreira de Oliveira, A.A.; Fonseca Saraiva, A.C.; de Oliveira, M.A.; Ishihara, J.H. Using hydrodynamic and water quality variables to assess eutrophication in a tropical hydroelectric reservoir. *J. Environ. Manag.* **2020**, *256*, 109932. [[CrossRef](#)]
38. Shatwell, T.; Adrian, R.; Kirillin, G. Planktonic events may cause polymictic-dimictic regime shifts in temperate lakes. *Sci. Rep.* **2016**, *6*, 24361. [[CrossRef](#)]
39. Soranno, P.A.; Carpenter, S.R.; Lathrop, R.C. Internal phosphorus loading in Lake Mendota: Response to external loads and weather. *Can. J. Fish. Aquat. Sci.* **1997**, *54*, 1883–1893. [[CrossRef](#)]
40. Mesman, J.P.; Ayala, A.I.; Goyette, S.; Kasparian, J.; Marcé, R.; Markensten, H.; Stelzer, J.A.A.; Thayne, M.W.; Thomas, M.K.; Pierson, D.C.; et al. Drivers of phytoplankton responses to summer wind events in a stratified lake: A modeling study. *Limnol. Oceanogr.* **2022**, *67*, 856–873. [[CrossRef](#)]
41. Lewis Jr., W. Biogeochemistry of tropical lakes. *Int. Ver. fÜR Theor. Angew. Limnol. Verh.* **2010**, *30*, 1595–1603. [[CrossRef](#)]
42. Sterner, R.W. On the Phosphorus Limitation Paradigm for Lakes. *Int. Rev. Hydrobiol.* **2008**, *93*, 433–445. [[CrossRef](#)]
43. Caputo, L.; Naselli-Flores, L.; Ordoñez, J.; Armengol, J. Phytoplankton distribution along trophic gradients within and among reservoirs in Catalonia (Spain). *Freshw. Biol.* **2008**, *53*, 2543–2556. [[CrossRef](#)]
44. Rychtecký, P.; Znachor, P. Spatial heterogeneity and seasonal succession of phytoplankton along the longitudinal gradient in a eutrophic reservoir. *Hydrobiologia* **2011**, *663*, 175–186. [[CrossRef](#)]
45. Gomes Nogueira, M. Phytoplankton composition, dominance and abundance as indicators of environmental compartmentalization in Jurumirim Reservoir (Paranapanema River), São Paulo, Brazil. *Hydrobiologia* **2000**, *431*, 115–128. [[CrossRef](#)]
46. Freire, R.; Calijuri, M.; Santaella, S. Longitudinal patterns and variations in water quality in a reservoir in the semiarid region of NE Brazil: Responses to hydrological and climatic changes. *Acta Limnol. Bras.* **2009**, *21*, 251–262.
47. de Moura-Júnior, E.G.; Severi, W.; Kamino, L.H.Y.; de Lemos-Filho, J.P. To what degree do spatial and limnological predictors explain the occurrence of a submerged macrophyte species in lotic and semi-lotic/lentic environments of a dammed river? *Limnology* **2021**, *22*, 101–110. [[CrossRef](#)]
48. Soomets, T.; Uudeberg, K.; Jakovels, D.; Brauns, A.; Zagars, M.; Kutser, T. Validation and Comparison of Water Quality Products in Baltic Lakes Using Sentinel-2 MSI and Sentinel-3 OLCI Data. *Sensors* **2020**, *20*, 742. [[CrossRef](#)]
49. Ogashawara, I.; Kiel, C.; Jechow, A.; Kohnert, K.; Ruhtz, T.; Grossart, H.-P.; Hölker, F.; Nejtgaard, J.C.; Berger, S.A.; Wollrab, S. The Use of Sentinel-2 for Chlorophyll-a Spatial Dynamics Assessment: A Comparative Study on Different Lakes in Northern Germany. *Remote Sens.* **2021**, *13*, 1542. [[CrossRef](#)]
50. Owens, E.M.; Effler, S.W.; O'Donnell, D.M.; Matthews, D.A. Modeling the Fate and Transport of Plunging Inflows to Onondaga Lake. *JAWRA J. Am. Water Resour. Assoc.* **2014**, *50*, 205–218. [[CrossRef](#)]
51. Sotiri, K.; Hilgert, S.; Mannich, M.; Bleninger, T.; Fuchs, S. Implementation of comparative detection approaches for the accurate assessment of sediment thickness and sediment volume in the Passaúna Reservoir. *J. Environ. Manag.* **2021**, *287*, 112298. [[CrossRef](#)]
52. Marcon, L.; Sotiri, K.; Bleninger, T.; Lorke, A.; Männich, M.; Hilgert, S. Acoustic Mapping of Gas Stored in Sediments of Shallow Aquatic Systems Linked to Methane Production and Ebullition Patterns. *Front. Environ. Sci.* **2022**, *10*. [[CrossRef](#)]
53. Hutchinson, G.E. On the Relation between the Oxygen Deficit and the productivity and Typology of Lakes. *Int. Rev. Gesamten Hydrobiol. Hydrogr.* **1938**, *36*, 336–355. [[CrossRef](#)]
54. Müller, B.; Bryant, L.D.; Matzinger, A.; Wüest, A. Hypolimnetic Oxygen Depletion in Eutrophic Lakes. *Environ. Sci. Technol.* **2012**, *46*, 9964–9971. [[CrossRef](#)]
55. Carneiro, F.M.; Nabout, J.C.; Vieira, L.C.G.; Roland, F.; Bini, L.M. Determinants of chlorophyll-a concentration in tropical reservoirs. *Hydrobiologia* **2014**, *740*, 89–99. [[CrossRef](#)]
56. Chen, G.; Fang, X.; Devkota, J. Understanding flow dynamics and density currents in a river-reservoir system under upstream reservoir releases. *Hydrol. Sci. J.* **2016**, *61*, 2411–2426. [[CrossRef](#)]